Chinese Chemical Letters 34 (2023) 108153

Contents lists available at ScienceDirect

Chinese Chemical Letters

journal homepage: www.elsevier.com/locate/cclet

(Salen)osmium(VI) nitrides catalyzed glutathione depletion in chemotherapy

Wanqiong Huang[a], Chen Pan[a], Yongliang Huang[a], Tao Huang[a], Xiaonan Dong[a], Yunzhou Chen[b], Huatian Shi[b], Taichu Lau[c], Wailun Man[b,*], Wenxiu Ni[a,d,**]

[a] Department of Medicinal Chemistry, Shantou University Medical College, Shantou 515041, China
[b] Department of Chemistry, Hong Kong Baptist University, Hong Kong, China
[c] Department of Chemistry, City University of Hong Kong, Hong Kong, China
[d] Chemistry and Chemical Engineering Guangdong Laboratory, Shantou 515063, China

ARTICLE INFO

Article history:
Received 6 November 2022
Revised 13 January 2023
Accepted 13 January 2023
Available online 15 January 2023

Keywords:
Chemotherapy
Osmium complex
Glutathione depletion
Apoptosis
Autophagy

ABSTRACT

Glutathione depletion provides a promising strategy for the design of non-platinum anticancer drugs. Here we report a series of electrophilic (salen)osmium(VI) nitrides that react with glutathione to generate (salen)osmium(III) ammine compounds. *In vitro* studies indicate that these osmium(VI) nitrides show comparable cytotoxicity to cisplatin against various carcinoma. Mechanistic studies with the representative compound $[Os^{VI}(N)(L^H)(OH_2)](PF_6)$ (**1**, $L^H = N,N'$-bis(salicylidene)-*o*-cyclohexyldiamine dianion) suggest that **1** induces glutathione depletion, reactive oxygen species generation, endoplasmic reticulum stress, and in turn triggers death receptor-mediated apoptosis and autophagy in lung cancer cells. *In vivo* evaluations show that **1** can inhibit tumor xenograft growth effectively with no body weight drop.

In chemotherapy, over 50% of patients receive treatment from platinum-based compounds. Unfortunately, the rising drug-resistant cases of these platinum-based compounds in a broad spectrum of cancers, presumably due to the upregulated glutathione (GSH) level in cancer cells, have prompted the search for other non-platinum drugs [1–4]. Hence, GSH depletion has been postulated as a potential strategy in chemotherapy development [5–7]. GSH is a tripeptide, made up of glutamic acid, cysteine, and glycine, which is an important antioxidant in mammalian cells. The SH group in cysteine is easily oxidized and coupled to form the GSSG dimer (Fig. 1a).

The oxidation of thiol-containing compounds by metal nitrides (M≡N) is known. For example, Meyer *et al.* reported the reduction of the osmium(VI) nitrides, *cis*/*trans*-$[Os^{VI}(N)(tpy)Cl_2]^+$ (tpy = 2,2′:6′,2″-terpyridine) by thiols (RSH) to afford the corresponding osmium(IV) sulfilimido complexes, *cis*/*trans*-$[Os^{IV}(NSR)(tpy)Cl_2]$ [8]. On the other hand, the mechanism for the oxidation of RSH by a highly electrophilic (salen)ruthenium(VI) nitride, $[Ru^{VI}(N)(salen)(MeOH)]^+$ has been reported [9]. In addition, M≡N-catalyzed GSH depletion in cancer therapy has been reported recently. The high-valent compounds, $[Mn^{V}(N)(salen)]$ and $[Cr^{V}(N)(quinolinato)_2]$ react readily with GSH at the initial stage to induce cancer cell death [10,11]. The compounds, $[Os^{VI}(N)(phen)Cl_3]$ (phen = 1,10-phenanthroline and its derivatives) are potent breast cancer agents with promising antiproliferative properties, as reported by Lippard *et al.* [12–14]. Recently, Berger *et al.* made use of this compound and reported the reduction pathway by GSH *via* atomic telemetry and computational study [15]. We have been interested in the design of metallodrugs based on the Os^{VI}≡N platform. By incorporating various ancillary ligands, most of these osmium nitrides show promising *in vitro* and *in vivo* anticancer properties [16–20]. In particular, $Os^{VI}(N)(N_2O_2)Cl$ (N_2O_2 = 2,2′-[{[2-(diethylamino)ethyl]-imino}bis(methylene)]-bis[4,6-dimethyl-phenoate(2−)]) triggers liver cancer cell death *via* the apoptosis and oncosis pathway in which the latter mechanism was found to occur in osmium for the first time [16]. This neutral compound is not electrophilic enough to react with GSH. Inspired by the highly electrophilic $[Ru^{VI}(N)(salen)(MeOH)]^+$ [21,22]. We herein report a series of electrophilic (salen)osmium(VI) nitrides bearing the tetradentate Schiff base ligands with the general formula $[Os^{VI}(N)(L^R)(OH_2)]PF_6$ **1**–**4** (Fig. 1b). The synthesis and electrophilic reactivity of **1** have been previously reported [23,24].

Similar to the synthetic procedure of **1**, the preparation and characterization of **2**–**4** are listed in the experimental section in

* Corresponding author.
** Corresponding author at: Department of Medicinal Chemistry, Shantou University Medical College, Shantou 515041, China.
E-mail addresses: wlman118@hkbu.edu.hk (W. Man), wxni@stu.edu.cn (W. Ni).

https://doi.org/10.1016/j.cclet.2023.108153
1001-8417/

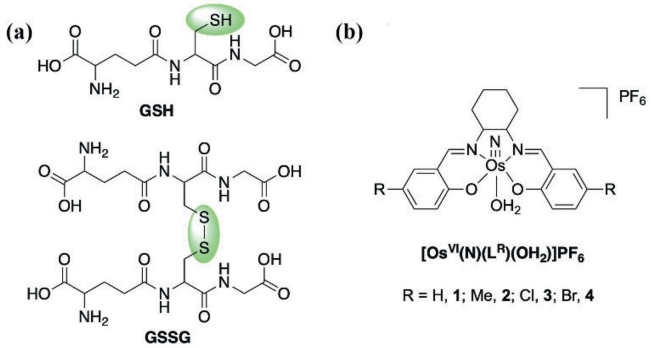

Fig. 1. The structures of (a) GSH and GSSG, and (b) **1**–**4**.

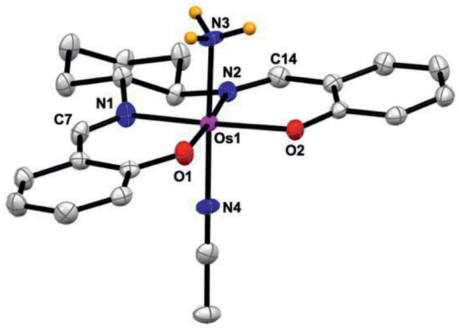

Fig. 2. Molecular structure of the cation of compound **5** with a partial atomic number scheme. Thermal ellipsoids are drawn at the 50% probability level. The solvent molecule and hydrogen atoms (except N3-H) are omitted for clarity.

Supporting information. We have also previously reported the synthesis of related osmium(VI) nitrido complexes that bear the ligand salophen (*N,N′*-bis(salicylidine)-*o*-phenylenediamine dianion) [25].

Compounds **1**–**4** are all cytotoxic towards different cancer cell lines, including the cisplatin-resistant cell line (A549DDP). In-depth *in vitro* studies indicated that **1** can deplete glutathione, trigger reactive oxygen species (ROS) accumulation, impair endoplasmic reticulum (ER) function, and initiate unfolded protein response to induce death receptor apoptosis and autophagy. *In vivo* antitumor evaluations also showed that **1** is a potent drug in effectively inhibiting tumor xenograft growth with no body weight loss.

The stability of **1**–**4** has been evaluated at 25 °C in various solutions by nuclear magnetic resonance (^{1}H NMR) and ultraviolet-visible spectroscopy (UV-vis). In neat DMSO, **1**–**4** are all stable for at least 24 h without notable spectral changes (Figs. S1 and S2 in Supporting information). In PBS solution (with 5% DMSO, PBS = phosphate-buffered saline, pH 7.0), only **1** is stable, while **2**–**4** show a significant UV–vis spectral change after 3 h (Fig. S3 in Supporting information).

Given that **1** is stable in PBS (with 5% DMSO), we further examined its stability towards some common biologically relevant reductants, such as ascorbic acid and GSH. **1** is a poor oxidant with a highly negative $Os^{VI/V}$ reduction potential (E_{pa} = –0.95 V *vs.* ferrocene in CH_3CN) [24]. As expected, it does not react with ascorbic acid (Fig. S4 in Supporting information). In contrast, the orange solution of **1** in 50% aqueous CH_3CN turned to dark red upon the addition of 10 equiv. GSH. Product analysis of the final red solution by electrospray ionization mass spectrometry (ESI-MS) indicates the formation of $[Os^{III}(NH_3)(L^H)(NCCH_3)]^+$ with a single peak at mass-to-charge (*m/z*) 570.5 (Fig. S5 in Supporting information). Other osmium(VI) nitrides also react with excess GSH to afford the corresponding ion $[Os^{III}(NH_3)(L^R)(NCCH_3)]^+$ (Fig. S6 in Supporting information). In a preparative scale, a dark red crystals of $[Os^{III}(NH_3)(L^H)(NCCH_3)](PF_6)$ (**5**) was isolated in moderate yield on standing the homogeneous solution containing **1** and 10 equiv. GSH in 50% aqueous CH_3CN for 2 d **5** was characterized by infrared (IR) and cyclic voltammetry (CV). The IR shows $\nu(NH_3)$ stretches at 3330 and 3168 cm^{-1} (Fig. S7 in Supporting information). The ruthenium analog, $[Ru^{III}(NH_3)(L^H)(NCCH_3)]PF_6$ exhibits $\nu(NH_3)$ bands at 3341, 3237 and 3135 cm^{-1} [9]. Similar $\nu(NH_3)$ bands were also reported in other osmium compounds such as $Os^{III}(NH_3)(Tp)Cl_2$ (3289, 3220 and 3156 cm^{-1}) and $[Os^{III}(NH_3)(tpm)Cl_2]^+$ (3338 and 3256 cm^{-1}) [where Tp = hydrodotris(1-pyrazolyl)borate anion and tpm = tris(1-pyrazolyl)methane] [26]. The CV of **5** in 0.1 mol/L $[^nBu_4N]PF_6$ in CH_3CN exhibits two reversible couples at +0.19 and –1.11 V (*vs.* ferrocene), which are assigned to $Os^{IV/III}$ and $Os^{III/II}$, respectively (Fig. S8 in Supporting information). The molecular structure of **5** was also determined by X-ray crystallography and depicted in Fig. 2. Selected bond angles are summarized in Table S1 (Supporting information). The detailed crystallographic data are summarized in Table S2 (Supporting information). Complexes **1** and **5** are isostructural with a distorted octahedral geometry. The most notable change is the elongation of the Os(1)–N(3) bond from 1.630(3) Å in **1** to 2.104(3) Å in **5**. The Os–NH_3 bond distance of **5** is slightly longer than that of the $[Ru^{III}(NH_3)(L^H)(NCCH_3)]^+$ analogue (2.083(4) Å) [9]. This Os–N bond elongation relieves the strong repulsion between the nitride and the salen plane. Hence, the elevated osmium center in **1** was pulled back to the mean equatorial salen plane in **5** with the four bond angles N(3)–Os(1)–N/O (donor atoms of the salen ligand) narrowed (Table S1, entries 1–4).

We have previously reported the mechanism for the reduction of $[Ru^{VI}(N)(L^H)(NCCH_3)]^+$ to $[Ru^{III}(NH_3)(L^H)(NCCH_3)]^+$ by thiols (RSH) (Scheme 1) [9]. The first step involves the nucleophilic addition of a RSH to the nitride to afford the diamagnetic ruthenium(IV) sulfilamido complex. This ruthenium(IV) species reacts further with 2 equiv. of RSH to produce $[Ru^{III}(NH_3)(L^H)(NCCH_3)]^+$ and releases 1.5 equiv. RSSR.

We speculated a similar reaction mechanism for the GSH reduction of **1** to **5**. Fig. 3 shows the time-dependent ^{1}H NMR spectra for the reaction between **1** and 10 equiv. GSH in CD_3CN-D_2O (v/v, 1:1). Pure **1** shows sharp and well-resolved signals for the imine and aromatic protons between δ 6.0 and 10.0. After the addition of 10 equiv. GSH, the two imine singlets at δ 9.13 and 8.93 of **1** gradually fade out. This is accompanied by the appearance of two distinct peaks at δ 9.41 and 9.33 ppm which are tentatively assigned to the imine protons of the osmium(IV) intermediate. The intensities of these two peaks reach a maximum after 15 min and then gradually decrease.

After 90 min only weak and broad signals (except the peak from GSH at δ 8.52) are observed, suggesting the formation of some paramagnetic species. This ^{1}H NMR result suggests the transformation of Os^{VI} (d^2 diamagnetic) → Os^{IV} (d^4 diamagnetic) → Os^{III} (d^5 paramagnetic), which is consistent with the mechanism for the reduction of $[Ru^{VI}(N)(L^H)(NCCH_3)]^+$ to $[Ru^{III}(NH_3)(L^H)(NCCH_3)]^+$ by thiols.

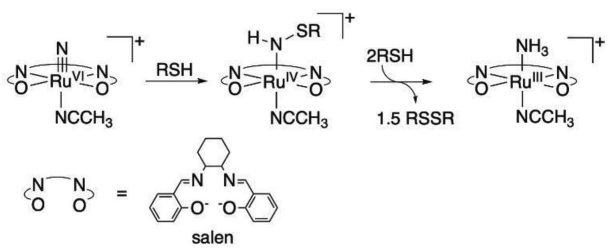

Scheme 1. Reduction of $[Ru^{VI}(N)(L^H)(NCCH_3)]^+$ by RSH.

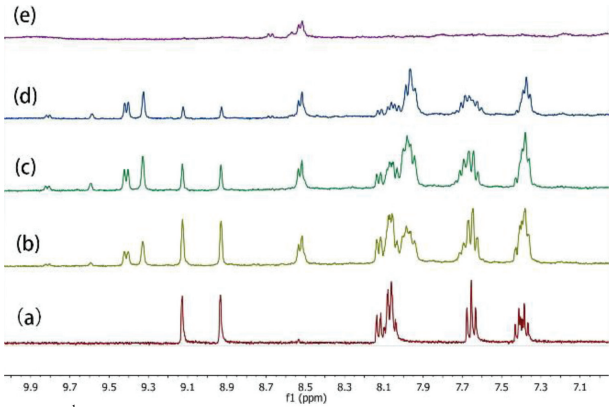

Fig. 3. ^{1}H NMR spectra for the reaction of 10 mmol/L **1** with 100 mmol/L GSH in CD_3CN-D_2O (v/v, 1:1) at different time intervals. (a) Before and after the addition of GSH at (b) 5 min, (c) 15 min, (d) 30 min, and (e) 90 min.

The *in vitro* antiproliferative activity of **1**–**4** toward various carcinoma, including lung (NCI-H460, A549 and A549DDP), liver hepatocellular (HepG2), cervical epithelioid (HeLa), ovarian (A2780), and breast (MDA-MB-231) has been evaluated using the MTT (3-(4,5-dimethylthiazol-2-yl)−2,5-diphenyltetrazolium bromide) method. The half inhibitory concentration (IC_{50}) values are summarized in Table 1. Amongst various carcinoma, **1** and **2** show comparable cytotoxicity to cisplatin with low IC_{50} values of 1.6–23.8 μmol/L. **3** and **4** can also inhibit the growth of cancer cells but have less cytotoxic potency. On the other hand, all **1**–**4** can inhibit the growth of cisplatin-resistant cells. The resistant factor (RF) value, derived from the ratio of IC_{50} values of A549DDP to that of A549, is low for **1** and **2** at 0.8 and 2.8, respectively. These RF values are significantly lower than that of cisplatin at 8.6 (Table 1, entry 3). More importantly, **1** is less cytotoxic toward normal liver cells (LO2) with the IC_{50} value of 53.1 μmol/L. The corresponding IC_{50} values for **2** and cisplatin are 7.5 and 5.0 μmol/L, respectively (Table 1, entry 8).

The cellular uptake efficiency of **1–4** in NCI-H460 cells after 6-h incubation has been evaluated by determining the intracellular osmium contents using inductively coupled plasma mass spectrometry (ICP-MS). All compounds exhibited concentration-dependent cellular accumulation (Fig. S9a in Supporting information). **1** and **2** showed in a higher cellular uptake, which is consistent with the above antiproliferative evaluation. We have further verified the cytotoxicity of **1** by colony formation assay (Fig. S9b in Supporting information). A 58% colony was formed in the 3.5 μmol/L **1**-treated NCI-H460 cells, while no colony formation was observed when the concentration of **1** was increased to 7.0 and 14.0 μmol/L. Among these osmium drugs, we have selected **1** as the representative compound for further biological studies because of its higher

Table 1
IC_{50} values of **1**–**4** and cisplatin against various cell lines.[a]

Entry	Cell line	1	2	3	4	Cisplatin
1	NCI-H460	7.0 ± 0.8	6.5 ± 0.3	44.9 ± 3.5	41.1 ± 5.7	7.4 ± 0.9
2	A549	23.8 ± 1.4	4.9 ± 0.7	45.3 ± 7.5	27.3 ± 2.9	12.3 ± 1.5
3	A549 DDP	19.1 ± 2.5	13.6 ± 0.5	52.6 ± 5.8	47.6 ± 3.4	105.9 ± 7.8
4	HeLa	13.9 ± 1.4	8.4 ± 0.5	43.4 ± 5.8	40.6 ± 3.4	13.6 ± 1.1
5	A2780	5.6 ± 1.2	1.6 ± 0.1	18.4 ± 1.8	8.3 ± 0.8	8.6 ± 0.2
6	MDA-MB-231	12.9 ± 2.0	6.0 ± 0.6	26.1 ± 3.3	25.4 ± 2.8	19.6 ± 1.3
7	HepG2	5.3 ± 0.5	1.7 ± 0.3	22.1 ± 0.4	7.6 ± 0.3	4.9 ± 0.3
8	LO2	53.1 ± 4.1	7.5 ± 0.5	67.8 ± 2.9	53.1 ± 9.1	5.0 ± 0.3

[a] IC_{50} values (μmol/L) are compound concentrations for 50% inhibition of cell viability after incubation for 48 h. Data are displayed as means standard deviations acquired in at least three independent experiments.

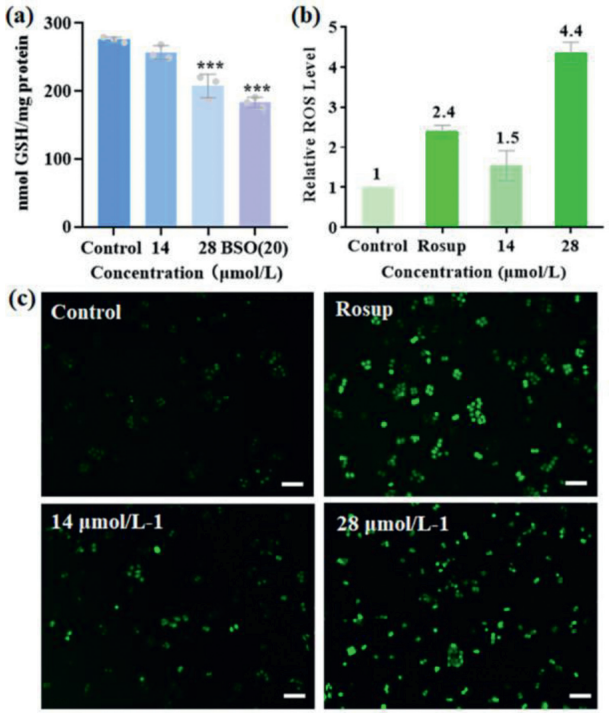

Fig. 4. (a) Intracellular GSH levels in NCI-H460 cells, $^{***}P < 0.001$. (b) Relative ROS levels in NCI-H460 cells. (c) Images of inverted fluorescence microscopy (scale bar = 50 μm).

stability and cytotoxicity. The GSH level is an indication and of great importance in controlling the redox system in mammalian cells. It acts as a scavenger to reduce ROS such as the superoxide (O_2^{-}) and hydroxyl radical ($HO^{\bullet}$) in cells [27,28]. As mentioned above, **1** was readily reduced by GSH to give **5**. This **1** → **5** transformation should have a great impact on the cellular GSH level and in turn the ROS level. First of all, we determined the cellular GSH level using monochlorobimane as the thiol probe. This thiol probe shows a weak fluorescence itself but it forms a strong fluorescent adduct when bound to GSH [29]. In the **1**-treated cells, a significant cellular GSH suppression was observed. Compared to control group, the GSH levels dropped by 7% and 25% in 14 and 28 μmol/L **1**-treated cells, respectively, and buthionine sulphoximine (BSO) was used as the positive control, (Fig. 4a). Next, we examined the cellular ROS expression using the fluorescent redox probe, 2′,7′-dichlorodihydrofluorescein diacetate (DCFH-DA) [30]. DCFH-DA itself is nonfluorescent and it readily converts to the highly fluorescent DCF in the presence of ROS [31]. Based on the fluorescence intensities determined by flow cytometry (Fig. 4b), the ROS accumulation enhancement was estimated to be 1.5 and 4.4 fold for the 14 and 28 μmol/L **1**-treated cells, respectively; which is further supported by the intensive green fluorescence images (Fig. 4c). In order to evaluate the effect of ROS, we determined the cell viability using the 24-h **1**-incubated NCI-H460 cells that have been pretreated with 5 mmol/L *N*-acetylcysteine (NAC) for 2 h (Fig. 5a). NAC is a well-known ROS scavenger which can capture ROS in cells. As expected, the drop in cell viability is inversely proportional to the concentration of **1**-treated cells. On the other hand, the cell viability with the NAC-pretreated cells is higher than the untreated cells in various concentrations of **1**-treated cells. These results indicate that **1** induced ROS-mediated cell death. The endoplasmic reticulum has recently emerged as a promising target for anticancer agents [32]. The enhancement of cellular ROS would induce ER stress and trigger programmed cell death *via* apoptosis and autophagy [27,33]. ER stress accumulates excessive unfolded

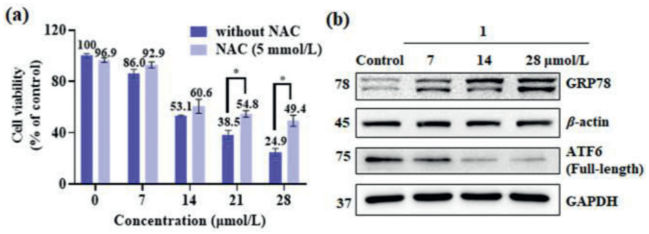

Fig. 5. (a) NCI-H460 cell viability for the 24-h incubation of **1** with untreated and 5 mmol/L NAC pretreated cells ($^{*}P < 0.05$ *vs.* control group; $^{**}P < 0.01$ *vs.* control group; $^{***}P < 0.001$ *vs.* control group). (b) Western blot analysis of GRP78 and ATF6 in 1-treated NCI-H460 cells.

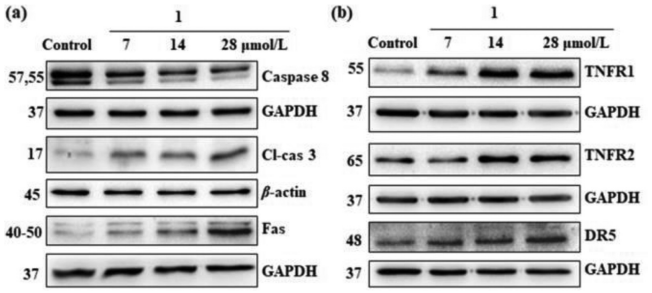

Fig. 7. WB analysis of remarkable proteins in **1**-treated NCI-H460 cells. (a) Caspase 8, cleaved-caspase 3 and Fas proteins, (b) TNFR1, TNFR2 and DR5 proteins.

or misfolded proteins in the ER lumen that will sequester the ER chaperone binding immunoglobin protein (GRP78) away from the ER stress sensor and activates transcription factor 6 (ATF6) [32–34]. As shown in Fig. 5b, the upregulation of GRP78 and the downregulation of ATF6 (full length) after a 24-h **1**-incubation indicate that **1** can impair ER function, initiate the unfolded protein response through ROS accumulation, and activate ATF6.

Apoptosis is the main cell death pathway for the action of metallodrugs in chemotherapy, which could be induced *via* the changes in intracellular GSH and ROS levels [28,35]. The flow cytometric analysis by Annexin V/PI double staining in **1**-treated NCI-H460 cells clearly shows that **1** activates apoptotic cell death (Fig. 6). The percentage for the sum of early (Q3-lower right) and late (Q2-upper right) apoptosis in untreated cells is 7.6%.

The percentage for the respective apoptosis increases gradually to 16.3%, 24.7%, and 31.6% for the 7, 14, and 28 μmol/L **1**-treated cells, respectively. Furthermore, the cell shrinkage morphology of NCI-H460 cells and enhanced blue fluorescence intensity in the apoptotic bodies after Hoechst 33258 staining further support the apoptotic cell death pathway (Fig. S10 in Supporting information). Apoptosis usually involves two major pathways, namely extrinsic and intrinsic pathways. The former pathway is death receptor-mediated while the latter pathway is mitochondrial-mediated [36]. Hence, we performed a series of Western blot (WB) assays using various remarkable proteins to figure out which apoptotic signal pathway is induced by **1**. The expression levels of proteins caspase 8 and cleaved-caspase 3 exhibited concentration-dependent decrease and enhancement respectively after treatment with **1** for 24 h (Fig. 7a). On the contrary, no notable change was observed in proteins caspase 9, Bcl-2 (pro-survival protein), and Bax (the pro-apoptosis protein) (Fig. S11a in Supporting information). These results suggest that the extrinsic pathway is more likely. This extrinsic pathway is further supported by the upregulated levels of other key proteins including TNFR1, TNFR2, Fas and DR5 (Fig. 7). Therefore, **1** mainly induces ROS-triggering death receptor-mediated apoptosis.

Interestingly, the down-regulated levels of FADD and TRADD in **1**-treated cells indicate the possibility of other cell death mechanisms (Fig. S11b in Supporting information). FADD is not only the adaptor protein for transmitting apoptotic signals, it is also implicated in autophagy cell death [37,38]. On the other hand, TRADD inhibition is also indicative of the possible autophagy mechanism [39]. Autophagy induced by rapid ROS accumulation and ER stress in cancer cells has been reported [40–42]. Hence, we performed the immunoblot assays using the widely used autophagy markers, proteins LC3 and p62 [43]. The dose-dependent elevated expression of p62 and upregulation of LC3BII/LC3BI suggest that **1** could induce cell death *via* autophagy (Fig. 8) [44]. Again, the reversed expression of procaspase 3 and p62 in **1**-induced NAC-pretreated cells suggest that **1** activates ROS mediated apoptosis and autophagy (Fig. S12 in Supporting information).

The efficacy of **1** and cisplatin on the growth of lung tumors was evaluated using nude mice model bearing NCI-H460. The animal experiments were approved by the Institutional Animal Care and Use Committee of Shantou University Medical College with the quality certificate No. 99005100012941. The License number is SYXK2017–0079 (Guangdong, China). Five groups of mice were randomly divided when the tumor volumes reached about 50 mm^3 (day 0). A tail intravenous (i.v.) injection was performed on days 0, 4, 8, 12, 16 and 20. The tumor volume and body weight of mice were measured each 2 days (Figs. 9a and b). At the end of the treatment (day 22), the tumor weight and size were determined (Figs. 9c and d). As expected, the cisplatin group (3 mg/kg) showed significant regression of tumor volume ($P < 0.005$) with respect to

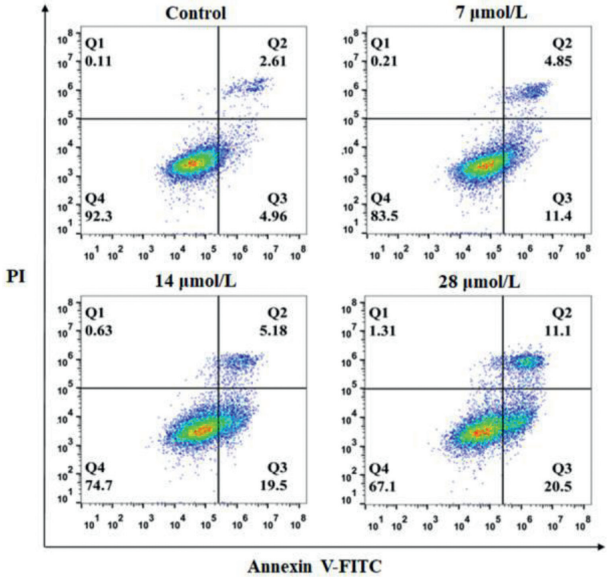

Fig. 6. Apoptosis effects of various concentrations of **1** on NCI-H460 cells.

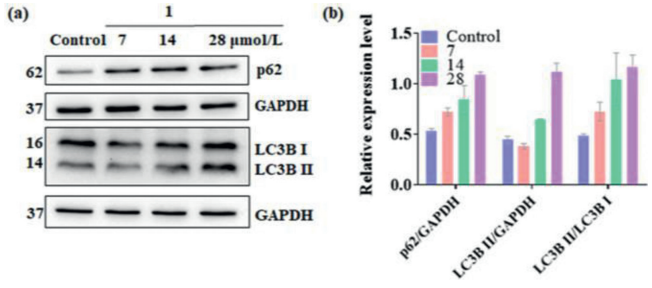

Fig. 8. (a) Immunoblot analysis of p62 and LC3B proteins in **1**-treated NCI-H460 cells. (b) Expression levels of p62 and LC3 proteins.

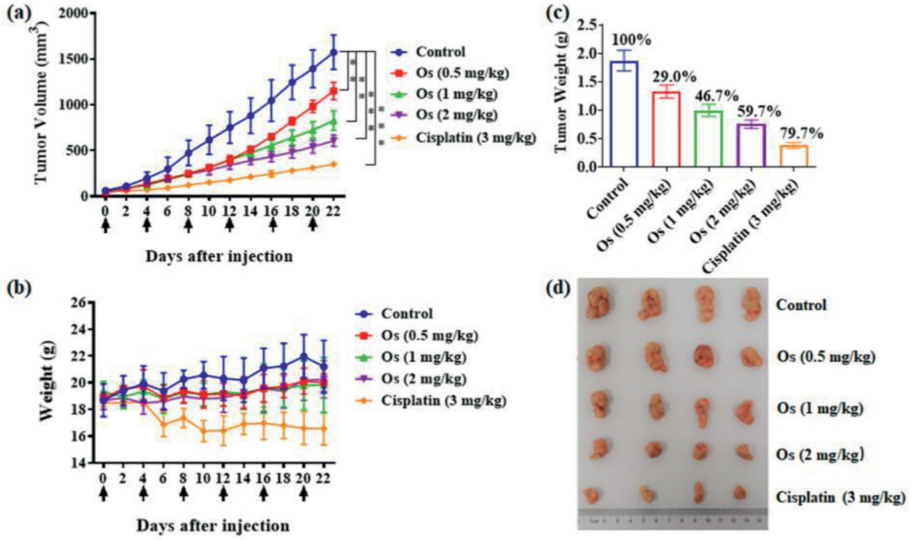

Fig. 9. Antitumor efficacy of **1** on NCI-H460 xenograft in nude mice (Os represents **1**). (a) The change in tumor volumes in different groups. $^{*}P < 0.05$ *vs.* control group; $^{**}P < 0.01$ *vs.* control group; $^{***}P < 0.001$ *vs.* control group. (b) The body weights of mice. (c) The final tumor weight at the end of treatment. (d) The images of the tumor tissues.

the control group. The inhibition rate of tumor weight was up to 79.7%. The mice groups treated with **1** also showed effective dose-dependent inhibition of tumor growth. The rates of tumor weight inhibition are 29.0%, 46.7% and 55.3% for the dosage of 0.5, 1 and 2 mg/kg **1**-treated groups, respectively. Unlike the cisplatin group, the nude mice grew steadily with no body weight drop for all **1**-treated groups during the therapy period.

In summary, we have demonstrated the remarkable multifunction of (salen)osmium(VI) nitrides **1**–**4** as potential chemotherapeutic agents. In particular, **1** shows selectivity towards a broad spectrum of carcinoma, including the cisplatin-resistant cell but not the normal liver cell. *In vitro*, **1** depletes intracellular GSH, resulting in elevated ROS generation to trigger ER stress and induces death receptor-mediated apoptosis and autophagy. *In vivo*, **1** displays effective inhibition of tumor growth with no body weight loss. This report of electrophilic osmium(VI) nitrides in depleting GSH should provide significant insight into the design of non-platinum drugs in chemotherapy.

Declaration of competing interest

The authors declared that they do not have any commercial or associative interest that represents a conflict of interest in connection with the work submitted.

Acknowledgments

This work was financially supported by the Guangdong Major Project of Basic and Applied Basic Research (No. 2019B030302009), the National Natural Science Foundation of China (No. 21401125), the Li Ka Shing Foundation Cross-Disciplinary Research Grant (No. 2020LKSFG01F), and Research Grants Council of Hong Kong (No. HKBU 12300121). W.L. Man thanks Hong Kong Baptist University for the start-up fund (No. RC-OFSGT2/20-21/SCI/008). This work is also supported by "Laboratory for Synthetic Chemistry and Chemical Biology" under the Health@InnoHK Program launched by Innovation and Technology Commission, The Government of Hong Kong Special Administrative Region of the People's Republic of China.

Supplementary materials

Supplementary material associated with this article can be found, in the online version, at doi:10.1016/j.cclet.2023.108153.

References

[1] L. Kelland, Nat. Rev. Cancer 7 (2007) 573–584.
[2] C. Huang, T. Li, J. Liang, et al., Coordin. Chem. Rev. 408 (2020) 213178–213193.
[3] X. Xiong, L.Y. Liu, Z.W. Mao, T. Zou, Coordin. Chem. Rev. 453 (2022) 214311–214339.
[4] A. Valente, A. Podolski-Renic, I. Poetsch, et al., Drug Resist. Updat. 58 (2021) 100778–100811.
[5] E. Desideri, F. Ciccarone, M.R. Ciriolo, Nutrients 11 (2019) 1926–1938.
[6] E. Falcone, A.G. Ritacca, S. Hager, et al., J. Am. Chem. Soc. 144 (2022) 14758–14768.
[7] X. Zhang, F. Ponte, E. Borfecchia, et al., Chem. Commun. 55 (2019) 14602–14605.
[8] P.S.White.M.V. Huynh, T.J. Meyer, J. Am. Chem. Soc. 123 (2001) 9170–9171.
[9] W.L. Man, W.W.Y. Lam, H.K. Kwong, et al., Inorg. Chem. 49 (2010) 73–81.
[10] H. Zhang, Y. Zhang, J. Cao, L. Ma, T. Chen, Chem. Commun. 58 (2022) 3759–3762.
[11] M. Chen, X. Huang, H. Shi, et al., Biomaterials 276 (2021) 120991–121001.
[12] K. Suntharalingam, T.C. Johnstone, P.M. Bruno, et al., J. Am. Chem. Soc. 135 (2013) 14060–14063.
[13] K. Suntharalingam, W. Lin, T.C. Johnstone, et al., J. Am. Chem. Soc. 136 (2014) 14413–14416.
[14] G. Berger, K. Grauwet, H. Zhang, et al., Cancer Lett. 416 (2018) 138–148.
[15] G. Berger, A. Wach, J. Sa, J. Szlachetko, Inorg. Chem. 60 (2021) 6663–6671.
[16] M. Ye, W.Q. Huang, Z.X. Li, et al., Chem. Commun. 58 (2022) 2468–2471.
[17] W.Q. Huang, C.X. Wang, T. Liu, et al., Dalton Trans. 49 (2020) 17173–17182.
[18] Q. Tang, W.X. Ni, C.F. Leung, et al., Chem. Commun. 49 (2013) 9980–9982.
[19] W.X. Ni, W.L. Man, S.M. Yiu, et al., Chem. Sci. 3 (2012) 1582.
[20] W.X. Ni, W.L. Man, M.T. Cheung, et al., Chem. Commun. 47 (2011) 2140–2142.
[21] T.M.L. Man, T.W. Wong, et al., J. Am. Chem. Soc. 126 (2004) 478–479.
[22] W.L. Man, W.W.Y. Lam, T.C. Lau, Acc. Chem. Res. 47 (2014) 427–439.
[23] W.L. Man, G. Chen, S.M. Yiu, et al., Dalton Trans. 39 (2010) 11163–11170.
[24] G. Chen, W.L. Man, S.M. Yiu, et al., Dalton Trans. 40 (2011) 1938–1944.
[25] T.W. Wong, T.C. Lau, W.T. Wong, Inorg. Chem. 38 (1999) 6181–6186.
[26] E.S. El-Samanody, K.D. Demadis, T.J. Meyer, P.S. White, Inorg. Chem. 40 (2001) 3677–3686.
[27] D. Trachootham, J. Alexandre, P. Huang, Nat. Rev. Drug Discov. 8 (2009) 579–591.
[28] Y. Xiong, C. Xiao, Z. Li, X. Yang, Chem. Soc. Rev. 50 (2021) 6013–6041.
[29] N.Kaplowitz JoséC.Fernández-Checa, Anal. Biochem. 190 (1990) 212–219.
[30] M. Yazdani, Toxicol. In Vitro 30 (2015) 578–582.
[31] S.L. Hempel, G.R. Buettner, Y.Q.O. Malley, D.A. Wessels, D.M. Flaherty, Free Radic. Biol. Med. 27 (1999) 146–159.
[32] A.P. King, J.J. Wilson, Chem. Soc. Rev. 49 (2020) 8113–8136.
[33] C. Hetz, Nat. Rev. Mol. Cell Biol. 13 (2012) 89–102.
[34] Y. Hotokezaka, I. Katayama, T. Nakamura, Commun. Biol. 3 (2020) 378.

[35] H.U. Simon, A. Haj-Yehia, F. Levi-Schaffer, Apoptosis 5 (2000) 415–418.
[36] M.S. D'Arcy, Cell Biol. Int. 43 (2019) 582–592.
[37] A. D'Anneo, D. Carlisi, M. Lauricella, et al., Cell Death Dis. 4 (2013) e891.
[38] L. Tourneur, G. Chiocchia, Trends Immunol. 31 (2010) 260–269.
[39] D. Xu, H. Zhao, M. Jin, et al., Nature 587 (2020) 133–138.
[40] X. Wen, J. Wu, F. Wang, et al., Free Radic. Biol. Med. 65 (2013) 402–410.
[41] C. Slator, Z. Molphy, V. McKee, A. Kellett, Redox Biol. 12 (2017) 150–161.
[42] C. Appenzeller-Herzog, M.N. Hall, Trends Cell Biol. 22 (2012) 274–282.
[43] N. Mizushima, T. Yoshimori, B. Levine, Cell 140 (2010) 313–326.
[44] N. Mizushima, A.M.Cuervo B.Levine, D.J. Klionsky, Nature 451 (2008) 1069–1075.